Int J Adv Manuf Technol (2017) 92:2299–2309
DOI 10.1007/s00170-017-0243-z

ORIGINAL ARTICLE

Third-order updated full-discretization method for milling stability prediction

Zhenghu Yan[1] · **Xibin Wang**[1] · **Zhibing Liu**[1] · **Dongqian Wang**[1] · **Li Jiao**[1] · **Yongjian Ji**[1]

Received: 2 October 2016 / Accepted: 6 March 2017 / Published online: 31 March 2017

Abstract Based on third-order Newton interpolation polynomial and direct integration scheme (DIS), this paper proposes a method to generate stability lobe diagram in milling process. The dynamic model of milling process with consideration of regeneration effect is described by time periodic delay-differential equation (DDE). Then, the DDE is rewritten as state space equation by a transformation. After equally discretizing the time delay into a series of small time intervals, the state space equation of milling system is integrated on the small time interval. Both the state term and delayed term are interpolated by third-order Newton interpolation polynomial, and the periodic-coefficient matrix is interpolated by first-order Newton interpolation polynomial. The state transition matrix which reflects the discrete mapping relation of dynamic responses for current tooth pass period and immediate previous tooth pass period is obtained directly. The accuracy of the proposed method is evaluated by comparing with benchmark methods in terms of the rate of convergence. The efficiency of the proposed method is verified through the comparison of computational time with existing methods. The proposed method is proved to be an accurate and efficient method by the comparison results. The distinction between up-milling and down-milling operations is also analyzed by comparing the stability lobe diagrams for these two operations. Besides, according to the analysis of rate of convergence, the number of substitutions, which are used to convert the variables located out of the required range into the required range, may affect the results of stability lobe diagrams. Moreover, the stability lobe diagram cannot be generated by using fourth-order updated full-discretization method.

Keywords Third-order Newton interpolation · Milling stability · Full-discretization · Regenerative effect · Rate of convergence

1 Introduction

With the rapid development of manufacturing industry, high-speed milling technology has an increasing demand for high-grade, precision and advanced products. However, regenerative chatter often occurs during high-speed milling operations. As many literatures mentioned, chatter is one of the most important limitations on the productivity of milling process [1]. It is detrimental to the formation of surface finish. Furthermore, it may shorten the life of cutting tool, and even shorten the life of machine tool. To gain high performance surface finish, chatter-free parameters should be selected for milling operations. Taking into account the regeneration effect, the dynamic model of milling process can be described by DDE [2, 3]. By solving the DDE, stability lobe diagram which indicates the relation between the axial depth of cut and the spindle speed of the machine tool can be obtained. The stability lobe diagram can be used to choose the proper parameters (spindle speed and axial depth of cut) for milling operations.

To our knowledge, a number of methods for chatter stability prediction in milling have been proposed. The first investigation of machine tool chatter and instabilities appeared at the beginning of the twentieth century as the result of metal removal process improvement [4]. Then, after the extensive works of Tlusty et al. [5] and Tobias [6], many attempts at chatter avoidance have been reported. Altintas et al. [7]

✉ Zhibing Liu
liuzhibing@bit.edu.cn

[1] Key Laboratory of Fundamental Science for Advanced Machining, School of Mechanical Engineering, Beijing Institute of Technology, Beijing 100081, China

proposed a zeroth-order approximation (ZOA) method which employs Fourier series components to approximate the time varying dynamic cutting force coefficients. However, this method is not suitable for low radial immersion conditions. To make ZOA method applicable to low radical immersion conditions, Merdol et al. [8] presented a multi-frequency method which utilizes higher-order harmonics of the Fourier series expansion to approximate the dynamic cutting force coefficients. Shorr et al. [9] developed a symbolic closed form solution for the analysis of dynamic stability of multiflute-end milling. Li et al. [10] employed the ratio of the predicted maximum dynamic cutting force to the predicted maximum static cutting force as a criterion for chatter stability analysis. They also considered the basic nonlinearity of the dynamic cutting process. In the literatures [5, 7, 8], the authors did not consider the nonlinear features of the milling system, therefore the resulting system of equations is linear. As for the nonlinear dynamics of milling process, Balachandran [11], Balachandran and Zhao [12] and Zhao and Balachandran [13] presented a unified-mechanics-based model, which allows for the regenerative effects and loss-of-contact effects. They also employed the reduced-order models to analyze the partial-immersion and full-immersion operations. Balachandran and Gilsinn [14] presented a mathematical model to study non-linear oscillations of milling process. In this model, the dependence of the time-delay effect on the feed rate is explained. They also pointed out that nonlinear models can be used to understand the nature of instability and post-instability motions. When ignoring the post-instability motions, the linear models are sufficient for predicting the milling stability, and they can be used to select proper machining parameters.

Since the linear models are useful for predicting the onset of chatter, there are a lot of researchers spending their efforts to develop numerical algorithms for predicting the milling stability. Bayly et al. [15] reported the temporal finite element analysis method which can be used to predict stability for arbitrary times in the cut. Butcher et al. [16] suggested the Chebyshev collocation method which utilizes the spectral differentiation matrix to approximate the derivatives of state term. Insperger and Stépán proposed the zeroth order semi-discretization method (othSDM) [17] and first-order semi-discretization method (1stSDM) [18] which respectively use the zeroth-order and first-order piecewise constant function to approximate the delayed term. Jin et al. [19] proposed an improved semi-discretization method to predict the stability lobes for variable pitch milling process. Li et al. [20] proposed a complete dicretization method for milling stability prediction. Xie et al. [21] developed an improved complete dicretization method to predict milling stability. In this method, most of the differential terms are discretized with Euler's method. Li et al. [22] proposed a Runge-Kutta-based method which is on the basis of the classical Runge-Kutta method and the complete dicretization method. Ozoegwu [23] proposed the third-order vector numerical integration method (3rdVNIM) and high-order VNIM to generate milling stability lobe diagrams.

Recently, Ding et al. [24] presented a full-discretization method (FDM) on the basis of DIS, which is found to be an efficient and widely used method. Then, different methods based on the DIS are proposed. Ding et al. developed the second-order full-discretization method [25] and numerical integration method [26] to calculate the stability boundary of the milling process. Liang et al. [27] reported an improved numerical integration method and extended this method to low radial immersion milling condition. Guo et al. [28] suggested a third-order full-discretization method which employs the third-order Newton interpolation polynomial to predict milling stability. Then, Guo et al. [29] modified the 3rdFDM to predict the stability lobes for non-uniform helix milling tools. Ozoegwu et al. reported the least squares approximation method [30] and hyper-third order full-discretization methods [31] to obtain the milling stability lobe diagrams. For the methods proposed in refs. [19–20, 23–26], only the state term is interpolated by higher-order interpolation polynomial. More recently, Tang et al. [32] proposed a second-order updated full-discretization method (2ndUFDM) for predicting milling stability. In this method, both the state term and delayed term are interpolated by second-order Lagrange interpolation polynomial. This method is proved to be an accurate and efficient method. Therefore, inspired by Tang's work [32] and Guo's work [29], this paper employs the third-order Newton interpolation polynomial to interpolate both the state term and delayed term in order to develop an accurate and efficient method for predicting milling stability. The focus of our paper is to propose a numerical algorithm for milling stability prediction to determine the onset of chatter, and analyze the computational efficiency and the rate of convergence of the proposed method.

The rest of this paper is organized as follows. In "Section 2", the mathematical model of milling dynamics is introduced. In "Section 3", milling stability analysis based on third-order updated full-discretization method (3rdUFDM) is presented. In "Section 4", the rate of convergence of the proposed method is analyzed by comparing with existing methods. In "Section 5", the stability lobe diagrams are generated, and the computational time of the proposed method is compared with the benchmark methods. Conclusions are drawn in "Section 6".

2 Mathematical model of milling process

In this section, the benchmark example for single degree of freedom-milling model is illustrated. The mathematical models of milling dynamics with consideration of the regenerative effect can be described by time periodic delay-differential equation as [17]

$$\ddot{x}(t) + 2\zeta\omega_n x(t) + \omega_n^2 x(t) = -\frac{a_p h(t)}{m}(x(t)-x(t-\tau)) \quad (1)$$

where ζ is the damping ratio, ω_n is the angular natural frequency, a_p is the axial depth of cut, m is the modal mass, $x(t)$ is the displacement in the current period, $x(t-\tau)$ is the displacement in the previous period, the time delay τ is equal to the tooth passing period T, and the instantaneous chip thickness $h(t)$ is defined as

$$h(t) = \sum_{j=1}^{N} g\left[\varphi_j(t)\right]\sin\left(\left(\varphi_j(t)\right)\right)\left[K_t\cos\left(\varphi_j(t)\right) + K_n\sin\left(\varphi_j(t)\right)\right] \quad (2)$$

where K_t, K_n are the tangential and the normal cutting force coefficients, respectively, N is the number of cutter tooth. The angular position of the jth tooth $\varphi_j(t)$ is determined as

$$\varphi_j(t) = (2\pi\Omega/60)t + (j-1)2\pi/N \quad (3)$$

where Ω denotes the spindle speed in rpm.

The function $g[\varphi_j(t)]$ is a window function which determines whether the tooth is in or out of cut. It is defined as

$$g\left[\varphi_j(t)\right] = \begin{cases} 1 & \text{if } \varphi_{st} < \varphi_j(t) < \varphi_{ex} \\ 0 & \text{otherwise} \end{cases} \quad (4)$$

where φ_{st} and φ_{ex} are the start and exit angles of the jth cutter tooth, respectively. For up-milling, $\phi_{st} = 0$ and $\varphi_{ex} = \arccos(1 - 2a_e/D)$; for down-milling, $\varphi_{st} = \arccos(2a_e/D - 1)$ and $\varphi_{ex} = \pi$, D is the diameter of cutter, a_e is the radial depth of cut. When the angular position of the jth cutting flute $\varphi_j(t)$ is between φ_{st} and φ_{ex}, the cutting flute is considered to be engaged with the workpiece, otherwise, the cutting flute is considered to be out of cut.

By using the transformation $\mathbf{x}(t) = [x(t)\ mx(t) + m\zeta\omega_n x(t)]$, Eq. (1) can be rewritten in the state space form as

$$\dot{\mathrm{x}}(t) = \mathrm{A}_0\mathrm{x}(t) + \mathrm{B}(t)\mathrm{x}(t) - \mathrm{B}(t)\mathrm{x}(t-\tau) \quad (5)$$

where $\mathrm{A}_0 = \begin{bmatrix} -\zeta\omega_n & \frac{1}{m} \\ m(\zeta\omega_n)^2 - m\omega_n^2 & -\zeta\omega_n \end{bmatrix}$ is a constant matrix, $\mathrm{B}(t) = [0 \quad 0 \quad -a_p h(t)\ 0]$ is a periodic-coefficient matrix with $\mathrm{B}(t) = \mathrm{B}(t+T)$.

In order to solve Eq. (5) numerically based on DIS, the first step is to divide the period T into n equal small time intervals with the length of h, that is $T = nh$, where n is an integer. Eq. (5) is integrated on the ith small time interval $[ih, (i+1)h]$, the result is

$$\mathrm{x}(t) = e^{\mathrm{A}_0(t-ih)}\mathrm{x}(ih) + \int_{ih}^{t} e^{\mathrm{A}_0(t-s)}\mathrm{B}(s)[\mathrm{x}(s) - \mathrm{x}(s-T)]ds \quad (6)$$

Eq. (6) can be equivalently express as [25]

$$\mathrm{x}(ih+h) = e^{\mathrm{A}_0 h}\mathrm{x}(ih) + \int_0^h e^{\mathrm{A}_0 s}\left[\mathrm{B}(ih+h-s)[\mathrm{x}(ih+h-s) - \mathrm{x}(ih+h-s-T)]ds \quad (7)\right.$$

Then, third-order updated full-discretization method is developed to numerically solve Eq. (7) with the aim of generating more accurate milling stability boundary.

3 Third-order updated full-discretization method

In the third-order updated full-discretization method (3rdUFDM), the state term $\mathrm{x}(ih+h-s)$ and delayed term $\mathrm{x}(ih+h-s-T)$ are both interpolated by third-order Newton interpolation polynomial. In the interpolation process, the nodal values $\mathrm{x}(ih-2h)$, $\mathrm{x}(ih-h)$, $\mathrm{x}(ih)$, and $\mathrm{x}(ih+h)$ denoted as x_{i-2}, x_{i-1}, x_i, and x_{i+1}, respectively, are employed to interpolate $\mathrm{x}(ih+h-s)$; the nodal values $\mathrm{x}(ih-T)$, $\mathrm{x}(ih+h-T)$, $\mathrm{x}(ih+2h-T)$, and $\mathrm{x}(ih+3h-T)$ denoted as x_{i-n}, x_{i-n+1}, x_{i-n+2}, and x_{i-n+3}, respectively, are employed to interpolate $\mathrm{x}(ih+h-s-T)$. Tang et al. [32] pointed out that high-order interpolation of periodic-coefficient matrix $\mathrm{B}(ih+h-s)$ has no apparent effect on improving effectiveness and efficiency compared to high-order interpolation of $\mathrm{x}(ih+h-s)$ and $\mathrm{x}(ih+h-s-T)$. Hence, $\mathrm{B}(ih+h-s)$ is interpolated by one-order Newton interpolation polynomial using the nodal values $\mathrm{B}(ih)$ and $\mathrm{B}(ih+h)$, which are denoted as B_i and B_{i+1}, respectively.

By using third-order Newton interpolation method, the state term $\mathrm{x}(ih+h-s)$ can be obtained and expressed as

$$\mathrm{x}(ih+h-s) \approx a_1\mathrm{x}_{i-2} + b_1\mathrm{x}_{i-1} + c_1\mathrm{x}_i + d_1\mathrm{x}_{i+1} \quad (8)$$

where

$$a_1 = \frac{s}{3h} - \frac{s^2}{2h^2} + \frac{s^3}{6h^3},\quad b_1 = \frac{-3s}{2h} + \frac{2s^2}{h^2} - \frac{s^3}{2h^3},\quad c_1 = \frac{3s}{h} - \frac{5s^2}{2h^2} + \frac{s^3}{2h^3},\quad d_1 = 1 - \frac{11s}{6h} + \frac{s^2}{h^2} - \frac{s^3}{6h^3} \quad (9)$$

The delayed term $\mathrm{x}(ih+h-s-T)$ is also obtained by third-order Newton interpolation method and expressed as

$$\mathrm{x}(ih+h-s-T) \approx a_2\mathrm{x}_{i-n} + b_2\mathrm{x}_{i-n+1} + c_2\mathrm{x}_{i-n+2} + d_2\mathrm{x}_{i+n+3} \quad (10)$$

$$a_2 = \frac{s}{3h} + \frac{s^2}{2h^2} + \frac{s^3}{6h^3}, \quad b_2 = 1 + \frac{s}{2h} - \frac{s^2}{h^2} - \frac{s^3}{2h^3},$$
$$c_2 = \frac{-s}{h} + \frac{s^2}{2h^2} + \frac{s^3}{2h^3}, \quad d_2 = \frac{s}{6h} - \frac{s^3}{6h^3} \tag{11}$$

The periodic-coefficient matrix $B(ih + h - s)$ is interpolated by first-order Newton interpolation method with the same expression as [24]:

$$B(ih + h - s) \approx B_{i+1} + \frac{(B_i - B_{i+1})s}{h} \tag{12}$$

substituting Eqs. (8–12) into Eq. (7) yields

$$M_{i,-2}x_{i-2} + M_{i,-1}x_{i-1} + (M_{i,0} + F_0)x_i + (M_{i,1} - I)x_{i+1} = M_{i,n}x_{i-n} + M_{i,n-1}x_{i-n+1} + M_{i,n-2}x_{i-n+2} + M_{i,n-3}x_{i-n+3} \tag{13}$$

where

$$M_{i,-2} = \left(\frac{F_2}{3h} - \frac{5F_3}{6h^2} + \frac{2F_4}{3h^3} - \frac{F_5}{6h^4}\right)B_{i+1} + \left(\frac{F_3}{3h^2} - \frac{F_4}{2h^3} + \frac{F_5}{6h^4}\right)B_i \tag{14}$$

$$M_{i,-1} = \left(\frac{-3F_2}{2h} + \frac{7F_3}{2h^2} - \frac{5F_4}{2h^3} + \frac{F_5}{2h^4}\right)B_{i+1} + \left(\frac{-3F_3}{2h^2} + \frac{2F_4}{h^3} - \frac{F_5}{2h^4}\right)B_i \tag{15}$$

$$M_{i,0} = \left(\frac{3F_2}{h} - \frac{11F_3}{2h^2} + \frac{3F_4}{h^3} - \frac{F_5}{2h^4}\right)B_{i+1} + \left(\frac{3F_3}{h^2} - \frac{5F_4}{2h^3} + \frac{F_5}{2h^4}\right)B_i \tag{16}$$

$$M_{i,1} = \left(F_1 - \frac{17F_2}{6h} + \frac{17F_3}{6h^2} - \frac{7F_4}{6h^3} + \frac{F_5}{6h^4}\right)B_{i+1} + \left(\frac{F_2}{h} - \frac{11F_3}{6h^2} + \frac{F_4}{h^3} - \frac{F_5}{6h^4}\right)B_i \tag{17}$$

$$M_{i,n} = \left(\frac{F_2}{3h} + \frac{F_3}{6h^2} - \frac{F_4}{3h^3} - \frac{F_5}{6h^4}\right)B_{i+1} + \left(\frac{F_3}{3h^2} + \frac{F_4}{2h^3} + \frac{F_5}{6h^4}\right)B_i \tag{18}$$

$$M_{i,n-1} = \left(F_1 - \frac{F_2}{2h} - \frac{3F_3}{2h^2} + \frac{F_4}{2h^3} + \frac{F_5}{2h^4}\right)B_{i+1} + \left(\frac{F_2}{h} + \frac{F_3}{2h^2} - \frac{F_4}{h^3} - \frac{F_5}{2h^4}\right)B_i \tag{19}$$

$$M_{i,n-2} = \left(\frac{-F_2}{h} + \frac{3F_3}{2h^2} - \frac{F_5}{2h^4}\right)B_{i+1} + \left(\frac{-F_3}{h^2} + \frac{F_4}{2h^3} + \frac{F_5}{2h^4}\right)B_i \tag{20}$$

$$M_{i,n-3} = \left(\frac{F_2}{6h} - \frac{F_3}{6h^2} - \frac{F_4}{6h^3} + \frac{F_5}{6h^4}\right)B_{i+1} + \left(\frac{F_3}{6h^2} - \frac{F_5}{6h^4}\right)B_i \tag{21}$$

$\mathbf{F}_0$ is equal to $e^{\mathbf{A}0}$, $\mathbf{I}$ is the identity matrix. $\mathbf{F}_1$-$\mathbf{F}_5$ can be obtained by the following recurrence relations.

$$F_1 = A_0^{-1}(F_0 - I) \tag{22}$$
$$F_2 = A_0^{-1}(hF_0 - F_1) \tag{23}$$
$$F_3 = A_0^{-1}(h^2F_0 - 2F_2) \tag{24}$$
$$F_4 = A_0^{-1}(h^3F_0 - 3F_3) \tag{25}$$
$$F_5 = A_0^{-1}(h^4F_0 - 4F_4) \tag{26}$$

In Eq. (13), x_{i-2}, x_{i-1}, x_i, and x_{i+1} represent the dynamic responses in the current period, x_{i-n}, x_{i-n+1}, x_{i-n+2}, and x_{i-n+3} represent the dynamic responses in the previous period. In order to construct the one-to-one discrete mapping relation of the dynamic responses between current period and the immediate previous period directly, the number of the nodal values used for interpolating $x(ih + h - s)$ (i.e., Eq. (8)) and $x(ih + h - s - T)$ (i.e., Eq. (10)) should be the same. Additionally, in the calculation process, all the variables '**x**' should be in two adjacent time periods (i.e., current period and the immediate previous period). If some of the variables '**x**' are located out of the required range of the current and immediate previous period, corresponding substitutions can be employed to convert them into required range.

As for Eq. (13), when $i = 1$, the left variables x_{i-2} and x_{i-1} of Eq. (13) are equal to x_{-1} and x_0, respectively. With the aim of constructing discrete mapping relation of dynamic responses between current period and immediate previous period conveniently, the variables x_{n-n-1} and x_{n-n} can be used to substitute x_{-1} and x_0, respectively. Consequently, Eq. (13) can be rewritten as

$$(M_{1,0} + F_0)x_1 + (M_{1,1} - I)x_2 = M_{1,n}x_{1-n} + M_{1,n-1}x_{2-n} + M_{1,n-2}x_{3-n} + M_{1,n-3}x_{4-n} - M_{1,-2}x_{n-n-1} - M_{1,-1}x_{n-n} \tag{27}$$

When $i = 2$, the left variable x_{i-2} of Eq. (13) is equal to x_0. Similarly, the variable x_{n-n} is used to substitute x_0. Then, Eq. (13) can be rewritten as

$$M_{2,-1}x_1 + (M_{2,0} + F_0)x_2 + (M_{2,1}-I)x_3 = M_{2,n}x_{2-n} + M_{2,n-1}x_{3-n} + M_{2,n-2}x_{4-n} + M_{2,n-3}x_{5-n} - M_{2,-2}x_{n-n} \quad (28)$$

when $i = n-1$, the right variable x_{i-n+3} is equal to x_2. With the substitution $x_2 = x_{n-n+2}$, Eq. (13) can be rewritten as

$$M_{n-1,-2}x_{n-3} + M_{n-1,-1}x_{n-2} + (M_{n-1,0} + F_0)x_{n-1} + (M_{n-1,1}-I)x_n - M_{n-1,n-3}x_2 = M_{n-1,n}x_{n-n-1} + M_{n-1,n-1}x_{n-n} + M_{n-1,n-2}x_{i-n+1} \quad (29)$$

when $i = n$, the right variable x_{i-n+3} is equal to x_3. With the substitution $x_3 = x_{n-n+3}$, Eq. (13) can be rewritten as

$$M_{n,-2}x_{n-2} + M_{n,-1}x_{n-1} + (M_{n,0} + F_0)x_n + (M_{n,1}-I)x_{n+1} - M_{n,n-2}x_2 - M_{n,n-3}x_3 = M_{n,n}x_{i-n} + M_{n,n-1}x_{n-n+1} \quad (30)$$

combining Eq. (13) and Eqs. (27–30), the discrete mapping relation of the dynamic responses between current period and the immediate previous period is obtained as

$$D_1 \begin{bmatrix} x_1 \\ x_2 \\ \vdots \\ \vdots \\ x_n \\ x_{n+1} \end{bmatrix} = D_2 \begin{bmatrix} x_{1-n} \\ x_{2-n} \\ \vdots \\ \vdots \\ x_{n-n} \\ x_{n-n+1} \end{bmatrix} \quad (31)$$

where

$$D_1 = \begin{bmatrix} I & 0 & 0 & 0 & \cdots & 0 & 0 & 0 & 0 & 0 & 0 \\ M_{1,0}+F_0 & M_{1,1}-I & 0 & 0 & \cdots & 0 & 0 & 0 & 0 & 0 & 0 \\ M_{2,-1} & M_{2,0}+F_0 & M_{2,1}-I & 0 & \cdots & 0 & 0 & 0 & 0 & 0 & 0 \\ M_{3,-2} & M_{3,-1} & M_{3,0}+F_0 & M_{3,1}-I & \cdots & 0 & 0 & 0 & 0 & 0 & 0 \\ \vdots & \vdots & \vdots & \vdots & \ddots & \vdots & \vdots & \vdots & \vdots & \vdots & \vdots \\ 0 & 0 & 0 & 0 & \cdots & M_{n-2,-2} & M_{n-2,-1} & M_{n-2,0}+F_0 & M_{n-2,1}-I & 0 & 0 \\ 0 & -M_{n-1,n-3} & 0 & 0 & \cdots & 0 & M_{n-1,-2} & M_{n-1,-1} & M_{n-1,0}+F_0 & M_{n-1,1}-I & 0 \\ 0 & -M_{n,n-2} & -M_{n,n-3} & 0 & \cdots & 0 & 0 & M_{n,-2} & M_{n,-1} & M_{n,0}+F_0 & M_{n,1}-I \end{bmatrix}$$

$$D_2 = \begin{bmatrix} 0 & 0 & 0 & 0 & 0 & 0 & \cdots & 0 & 0 & 0 & I \\ M_{1,n} & M_{1,n-1} & M_{1,n-2} & M_{1,n-3} & 0 & 0 & \cdots & 0 & -M_{1,-2} & -M_{1,-1} & 0 \\ 0 & M_{2,n} & M_{2,n-1} & M_{2,n-2} & M_{2,n-3} & 0 & \cdots & 0 & 0 & -M_{2,-2} & 0 \\ 0 & 0 & M_{3,n} & M_{3,n-1} & M_{3,n-2} & M_{3,n-3} & \cdots & 0 & 0 & 0 & 0 \\ \vdots & \vdots & \vdots & \vdots & \vdots & \vdots & \ddots & \vdots & \vdots & \vdots & \vdots \\ 0 & 0 & 0 & 0 & 0 & 0 & \cdots & M_{n-2,n} & M_{n-2,n-1} & M_{n-2,n-2} & M_{n-2,n-3} \\ 0 & 0 & 0 & 0 & 0 & 0 & \cdots & 0 & M_{n-1,n} & M_{n-1,n-1} & M_{n-1,n-2} \\ 0 & 0 & 0 & 0 & 0 & 0 & \cdots & 0 & 0 & M_{n,n} & M_{n,n-1} \end{bmatrix}$$

If $\mathbf{D}_1$ is a nonsingular matrix, the state transition matrix $\boldsymbol{\psi}$ for the dynamic system over one period T is written as

$$\psi = (D_1)^{-1}D_2 \quad (32)$$

Then, the stability of the dynamic system can be determined according to Floquet theory, the decision criterion is as follow:

$$\max(|\lambda(\boldsymbol{\psi})|)\begin{cases} < 1 & \text{stable} \\ = 1 & \text{critical stable} \\ > 1 & \text{unstable} \end{cases} \quad (33)$$

4 Rate of convergence

With the aim of illustrating the rate of convergence of the proposed method, the classical and widely used 1stSDM as well as the newly proposed 3rdVNIM and 2ndUFDM is taken as the benchmark method for comparing with the proposed 3rdUFDM.

The rate of convergence can be used to evaluate the local errors between the absolute value of the maximal critical eigenvalues of the state transition matrix $|\mu(n)|$ and the exact value μ_0, where $|\mu(n)|$ is a function of discrete number of the tooth passing period (i.e., n). μ_0 is not a strictly exact value, it is considered exact when the value of the parameter n is high enough. In this paper, μ_0 is determined by the 1stSDM with

n = 200. To demonstrate the rate of convergence of the 3rdUFDM, the radial depth of cut ratio is set as a_e/D=1 to avoid intermittent milling, the spindle speed is Ω = 5000 rpm, and the axial depth of cuts are chosen as a_p=0.1, 0.4, 0.7 and 1.0 mm, respectively.

The program is conducted using Matlab 2010a software on a computer with Intel (R) Core (TM) i3-3120 and 2 GB memory. In this paper, most of the machining parameters are chosen as the same as [17] to calculate the rate of convergence of different methods. The parameters are the number of tooth N = 2, the angle natural frequency ω_n=2π × 922 rad/s, the relative damping is ζ=0.011, the modal mass is m = 0.03993 kg, the cutting force coefficients are K_t=6 × 10^8 N/m^2, and K_n = 2 × 10^8, down milling. The rates of convergence for different methods with different computational parameters n are illustrated in Fig. 1.

As shown in Fig. 1a, 3rdUFDM converges faster than 2ndUFDM, while in Fig. 1b–d, 2ndUFDM converges a little faster than 3rdUFDM. It is indicated from Fig. 1 that 3rdUFDM has a more apparent advantage with a smaller axial depth of cut. Meanwhile, it is seen from Fig. 1c that the local errors calculated by 3rdUFDM are smaller than that calculated by 2ndUFDM when n is greater than 63. Similarly, according to Fig. 1d, the local errors calculated by 3rdUFDM are smaller than that calculated by 2ndUFDM when n is greater than 56. Therefore, it is concluded that both the 2ndUFDM and 3rdUFDM have their own advantages. Generally, these two updated methods converge faster to a stable state than other methods.

In mathematical theory, the higher rate of convergence can be obtained by using higher-order interpolation methods. However, only in Fig. 1a, the 3rdUFDM converges faster than 2ndUFDM; in Fig. 1b–d, 2ndUFDM converges a little faster than 3rdUFDM. This may be caused by the number of substitutions which are used in calculation process to convert the variables located out of the required range into the required range. It is indicated from Eq. (31) that the required range of dynamic response for current period is between x_1 and x_{n+1}, i.e., [x_1, x_2, ⋯, x_n, x_{n+1}], and the required range of dynamic response for immediate previous period is between x_{1-n} and x_{n-n+1}, i.e., [x_{1-n}, x_{2-n}, ⋯, x_{n-n}, x_{n-n+1}]. In 2ndUFDM [32], the variables x_0 and x_{n-n+2} are located out of the required range. With the aim of constructing discrete mapping relation of the dynamic responses between current

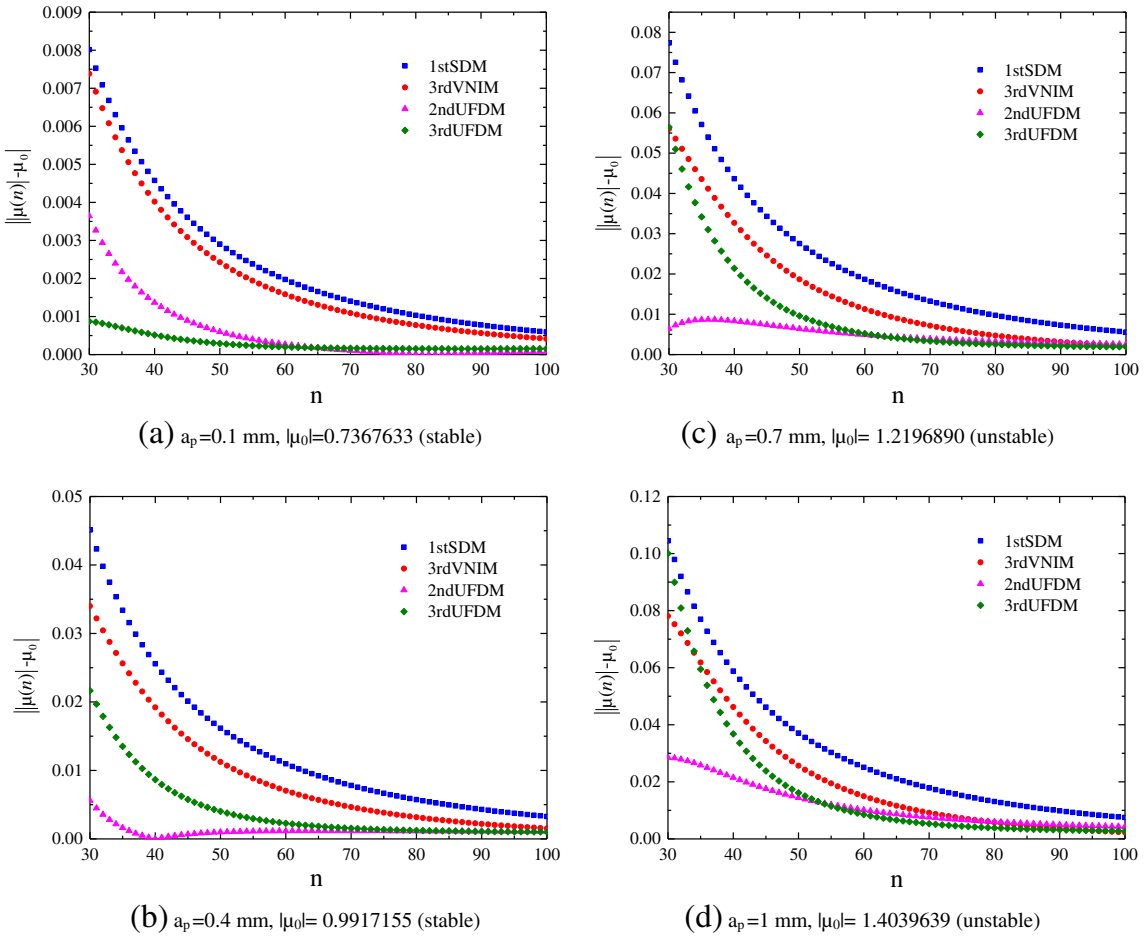

Fig. 1 Convergences of the critical eigenvalues with different computation parameter n for 1stSDM, 3rdVNIM, 2ndUFDM, and the proposed method. **a** a_p = 0.1 mm, $|\mu_0|$ = 0.7367633 (stable); **b** a_p = 0.4 mm, $|\mu_0|$ = 0.9917155 (stable); **c** a_p = 0.7 mm, $|\mu_0|$ = 1.2196890 (unstable); **d** a_p = 1 mm, $|\mu_0|$ = 1.4039639 (unstable)

period and immediate previous period, two substitutions, i.e., $x_{n-n} = x_0$, $x_2 = x_{n-n+2}$, are used in the calculation process. In 3rdUFDM, the variables x_{-1}, x_0, x_{n-n+2} and x_{n-n+3} are located out of the required range, and four substitutions, i.e., $x_{n-n-1} = x_{-1}$, $x_{n-n} = x_0$, $x_2 = x_{n-n+2}$ and $x_3 = x_{n-n+3}$, are used in the calculation process. These substitutions are useful for constructing discrete mapping relations of the dynamic responses between current period and immediate previous period, but they may affect the result of state transition matrix ψ, and thus affect the result of stability lobe diagram.

The authors also try to use the fourth-order Newton interpolation method to solve the DDE. The state term $x(ih + h - s)$ are interpolated by nodal values x_{i-3}, x_{i-2}, x_{i-1}, x_i, and x_{i+1}, and the delayed term $x(ih + h - s - T)$ are interpolated by nodal values x_{i-n}, x_{i-n+1}, x_{i-n+2}, x_{i-n+3}, and x_{i-n+4}. In the calculation process, six substitutions $x_{n-n-2} = x_{-2}$, $x_{n-n-1} = x_{-1}$, $x_{n-n} = x_0$, $x_2 = x_{n-n+2}$, $x_3 = x_{n-n+3}$, and $x_4 = x_{n-n+4}$ are used to obtain the discrete mapping relations of the dynamic responses between current period and immediate previous period. However, the stability lobe diagrams cannot be generated finally.

From Fig. 1b–d, it should be noted that the local errors calculated by 3rdUFDM decrease with the increase of parameter n. The local errors calculated by 3rdUFDM are smaller than that calculated by other methods when n is close to 100. Therefore, it can be inferred from Fig. 1 that the influence of

Table 1 Stability lobe diagrams obtained by the 1stSDM, 3rdVNIM, 2ndUFDM and 3rdUFDM for down-milling operation

Methods	$n = 30$, $a_e/D = 0.1$	$n = 40$, $a_e/D = 0.5$	$n = 50$, $a_e/D = 1$
1stSDM	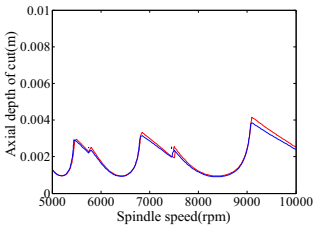	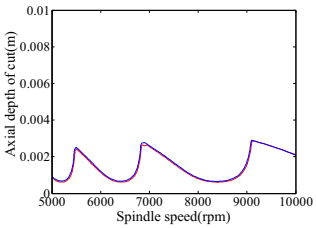	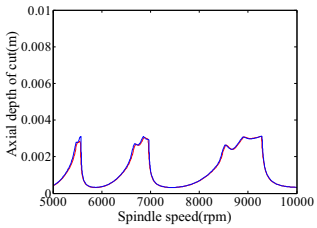
	100 s	151 s	222 s
3rdVNIM	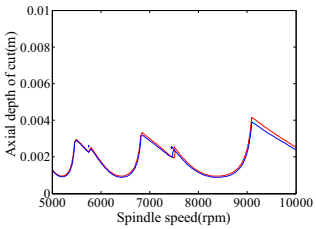	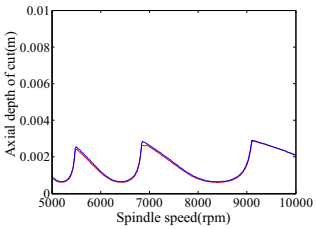	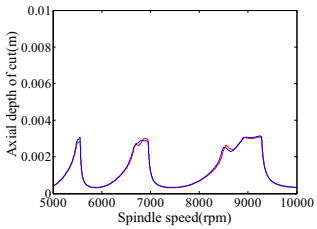
	111 s	166 s	241 s
2ndUFDM	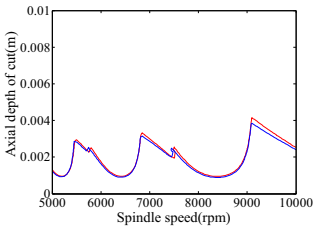	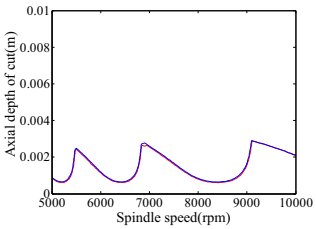	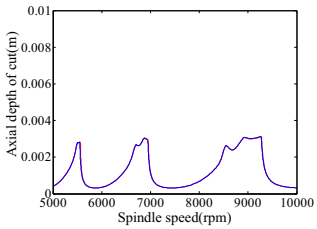
	25 s	45 s	73 s
3rdUFDM	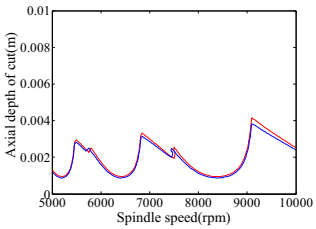	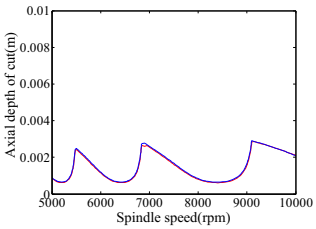	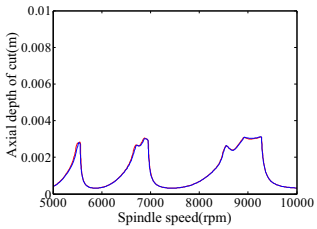
	27 s	51 s	81 s

the number of substitutions used in calculation process on the state transition matrix ψ and the results of stability lobe diagrams becomes smaller with the increase of parameter n.

5 Stability lobe diagrams

In order to illustrate the computational efficiency of the proposed method, the stability lobe diagrams obtained by 3rdUFDM are compared with that obtained by 1stSDM, 3rdVNIM, and 2ndUFDM. The stability charts are calculated over 100 × 100 sized equidistance grid with the spindle speed ranging from 5×10^3 to 10×10^3 rpm, and the axial depth of cut ranging from 0 to 0.01 m. The radial immersion ratio a_e/D is set as 0.1, 0.5, and 1, and the corresponding parameter n is chosen as 30, 40, and 50 to generate stability lobe diagrams, respectively. The stability lobe diagrams calculated by 1stSDM with $n = 100$ is taken as the ideal ones. In the stability charts, the ideal stability lobe diagrams are denoted with red line curves, and the actual stability lobe diagrams are denoted with blue line curves. In this work, the stability lobe diagrams for both down-milling and up-milling operations are obtained. The stability lobe diagrams obtained by 1stSDM, 3rdVNIM, 2ndUFDM, and 3rdUFDM for down-milling operation are listed in Table. 1.

It is seen from Table 1 that the stability lobe diagrams obtained by 3rdUFDM for down-milling operation are almost identical to that obtained by 2ndUFDM. Both 2ndUFDM and 3rdUFDM can generate the stability lobe diagrams which are much closer to the ideal curves than 1stSDM and 3rdVNIM.

Table 2 Stability lobe diagrams obtained by 1stSDM, 3rdVNIM, 2ndUFDM, and 3rdUFDM for up-milling operation

Methods	$n=30$, $a_e/D=0.1$	$n=40$, $a_e/D=0.5$	$n=50$, $a_e/D=1$
1stSDM	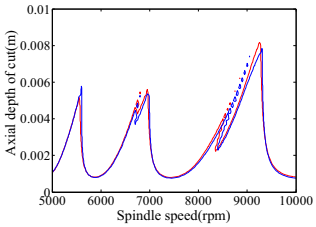	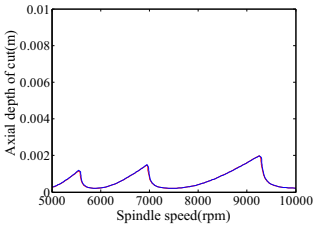	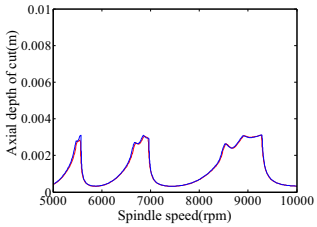
3rdVNIM	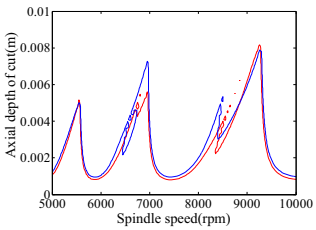	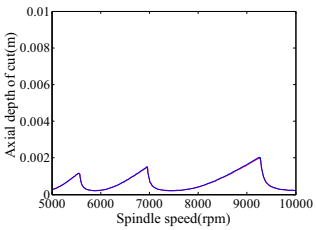	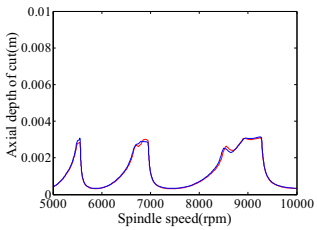
2ndUFDM	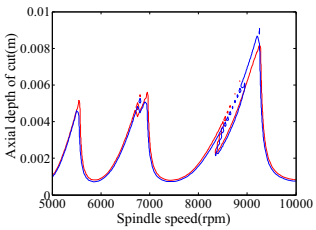	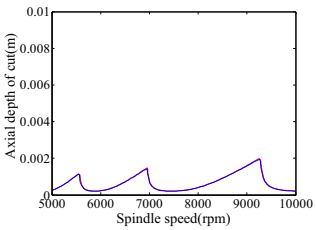	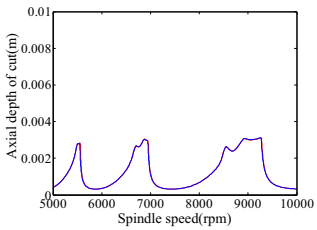
3rdUFDM	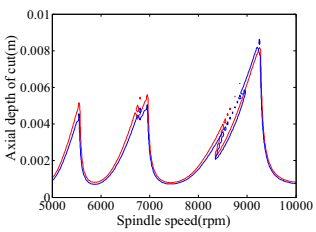	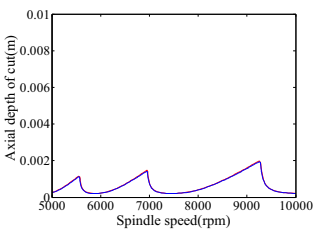	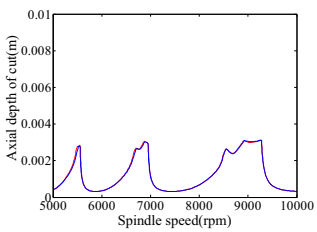

The computational time of 1stSDM, 3rdVNIM, 2ndUFDM, and 3rdUFDM for obtaining stability lobe diagrams with different radial immersion ratios are also listed in Table 1. It can be seen from Table 1 that the computational time of 1stSDM with $n = 30$, $n = 40$, and $n = 50$ for different radial immersion ratios is 100, 151, and 222 s, respectively. The corresponding computational time of 3rdVNIM is 111, 166, and 241 s. For the 2ndUFDM, the corresponding computational time is 25, 45, and 73 s. For the proposed method, the corresponding computational time is 27, 51, and 81 s. The proposed 3rdUFDM takes less time than 1stSDM and 3rdVNIM to generate stability lobe diagrams. The 2ndUFDM is proved to be an efficient method to predict milling stability. As observed in Table 1, according to the comparison in time cost between 3rdUFDM and 2ndUFDM, it is found that the increment of computational time between 3rdUFDM and 2ndUFDM is very small. Therefore, the 3rdUFDM is also an efficient method for stability prediction in milling.

The stability lobe diagrams for an up-milling operation are different from the stability lobe diagrams for a down-milling [11, 33]. In order to make a distinction between up-milling and down-milling operations, we also generate the stability lobe diagrams for an up-milling operation with the same radial immersion ratios and parameter n. The stability lobe diagrams obtained by 1stSDM, 3rdVNIM, 2ndUFDM, and 3rdUFDM for up-milling operation are listed in Table 2. We also get the computational time of the 1stSDM, 3rdVNIM, 2ndUFDM, and 3rdUFDM for up-milling operation. Because the computational time for up-milling operation is the same with that for down-milling operation, it is not listed in Table 2.

From Table 1 and Table 2, it can be seen that the stable range of axial depth of cut for up-milling is larger the stable range of axial depth of cut for down-milling when the radial immersion ratios a_e/D is set as 0.1. When the radial immersion ratios a_e/D is set as 0.5, the stable range of axial depth of cut for down-milling is a little larger that for down-milling. Besides, the peaks of the stability lobe for these two operations appear toward to opposite directions. The stability lobe diagrams for up-milling and down-milling are identical when the radial immersion ratios a_e/D is set as 1. For the partial immersion condition ($a_e/D = 0.1$ and $a_e/D = 0.5$), the stability lobe diagrams for up-milling and down-milling are different because the feed directions of these two operations are different. Accordingly, the start angle and the exit angle of cutter tooth for these two operations are different. For the full immersion condition ($a_e/D = 1$), the start angle and the exit angle of cutter tooth for up-milling and down-milling are the same, therefore, the stability lobe diagrams of these two operations are identical.

In order to demonstrate the predicted results of 3rdUFDM with a large value of parameter n, the stability lobe diagram obtained by the widely used 1stSDM with $n = 200$ is taken as

Table 3 Stability lobe diagrams of 3rdUFDM with $n = 70$, 80, 90, and 100

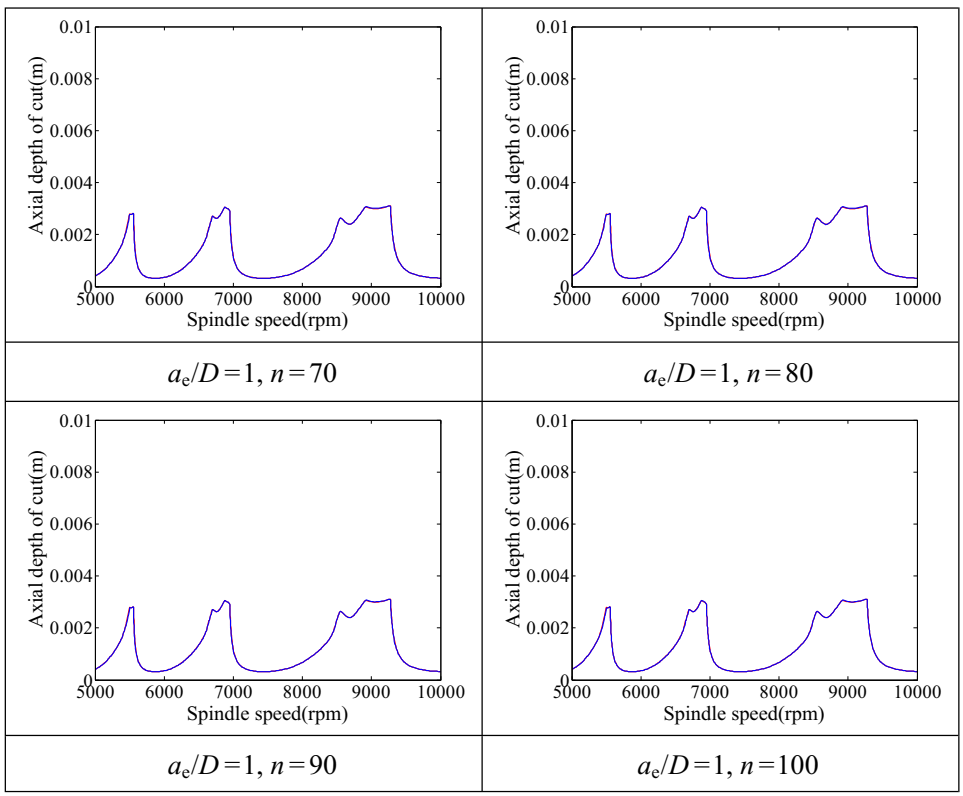

$a_e/D = 1$, $n = 70$ | $a_e/D = 1$, $n = 80$

$a_e/D = 1$, $n = 90$ | $a_e/D = 1$, $n = 100$

the criterion-referenced lobe diagram. The stability lobe diagrams with n = 70, 80, 90, and 100 are generated, as shown in Table 3.

It is seen from Table 3 that the stability lobe diagrams of 3rdUFDM with n = 70 are highly identical to that of 1stSDM with n = 200, which means the proposed 3rdUFDM is much more efficient than the widely used 1stSDM. The curves of stability lobe diagrams generated by 1stSDM with n = 200 are coved by that generated by 3rdUFDM with n = 80, 90, and 100.

6 Conclusions

The focus of this paper is to propose a third-order update full-discretization method for stability prediction in milling. The following conclusions can be drawn.

(1) The mathematical model of a single DOF milling system with consideration of regenerative effect is established. The dynamic equation of milling process is represented as DDE in state space form.

(2) The third-order Newton interpolation polynomials are used to interpolate both the state term $\mathbf{x}(ih + h\text{-}s)$ and delayed term $\mathbf{x}(ih + h\text{-}s\text{-}T)$, the first-order Newton interpolation polynomials are used to interpolate the periodic coefficient matrix $\mathbf{B}(ih + h\text{-}s)$. The state transition matrix $\boldsymbol{\psi}$ is obtained directly by solving the DDE based on DIS. In order to demonstrate the accuracy of the proposed method, the 1stSDM, 3rdVNIM, and 2ndUFDM are taken as the benchmark for comparing with the 3rdUFDM in terms of the rate of convergence. The 3rdUFDM has a more apparent advantage with a smaller axial depth of cut. Besides, the 3rdUFDM converges faster to a stable state than the benchmark 1stSDM and 3rdVNIM.

(3) By comparing 3rdUFDM with 2ndUFDM in terms of rate of convergence, it is found that the results of stability lobe diagram may be affected by the number of substitutions which are used to convert the variables located out of the required range into the required range. When n is close to a large value, it has little effect on the state transition matrix and the results of stability lobe diagrams.

(4) The computational time of the 3rdUFDM is compared with that of the 1stSDM, 3rdVNIM, and 2ndUFDM, the comparison results show that the 3rdUFDM takes less time to generate stability lobe diagram than 1stSDM and 3rdVNIM. In addition, the increment of computational time between 3rdUFDM and 2ndUFDM is very small. Therefore, the proposed 3rdUFDM is proved to be an efficient method. The distinction between up-milling and down-milling operations is also analyzed by comparing the stability lobe diagrams of these two operations.

Acknowledgements This work was partially supported by the National Natural Science Foundation of China (Grant No. 51375055 and No. 51575050).

References

1. Budak E (2006) Analytical models for high performance milling. Part II: Process dynamics and stability. Int J Mach Tools Manuf 46(12):1489–1499
2. Altintas Y (2000) Manufacturing automation: metal cutting mechanics, machine tool vibrations, and CNC design. Cambridge University Press, Cambridge
3. Altintas Y, Weck M (2004) Chatter stability of metal cutting and grinding. CIRP Ann-Manuf Techn 53(2):619–642. doi:10.1016/S0007-8506(07)60032-8
4. Quintana G, Ciurana J (2011) Chatter in machining process: a review. Int J Mach Tools Manuf 51(5):363–376. doi:10.1016/j.ijmachtools.2011.01.001
5. Tlusty J, Polacek A, Danek C, Spacek J (1962) Selbsterregte Schwingungen an Werkzeugmaschinen. VEB Verlag Technik, Berlin
6. Tobias SA (1965) Machine tool vibration. Blackie, London
7. Altintas Y, Budak E (1995) Analytical prediction of stability lobes in milling. CIRP Ann-Manuf Techn 44(1):357–362. doi:10.1016/S0007-8506(07)62342-7
8. Merdol SD, Altintas Y (2004) Multi frequency solution of chatter stability for low immersion milling. J Manuf Sci Eng 126(3):459–466. doi:10.1115/1.1765139
9. Shorr MJ, Liang SY (1996) Chatter stability analysis for end milling via convolution modeling. Int J Adv Manuf Technol 11(5):311–318. doi:10.1007/BF01845689
10. Li HZ, Li XP, Chen Q (2003) A novel chatter stability criterion for the modeling and simulation of the dynamic milling process in the time domain. Int J Adv Manuf Technol 22:619–625. doi:10.1007/s00170-003-1562-9
11. Balachandran B (2001) Nonlinear dynamics of milling processes. PHILOS T R SOC A 359(1781):793–819. doi:10.1098/rsta.2000.0755
12. Balachandran B, Zhao MX (2000) A mechanics based model for study of dynamics of milling operations. Meccanica 35(2):89–109. doi:10.1023/A:1004887301926
13. Zhao MX, Balachandran B (2001) Dynamics and stability of milling process. Int J Solids Struct 38(10):2233–2248. doi:10.1016/S0020-7683(00)00164-5
14. Balachandran B, Gilsinn D (2005) Non-linear oscillations of milling. Math Comp Model Dyn 11(3):273–290. doi:10.1080/13873950500076479
15. Bayly PV, Halley JE, Mann BP, Davies MA (2003) Stability of interrupted cutting by temporal finite element analysis. J Manuf Sci Eng 125(2):220–225. doi:10.1115/1.1556860
16. Butcher EA, Bobrenkov OA, Bueler E, Nindujarla P (2009) Analysis of milling stability by the Chebyshev collocation method: algorithm and optimal stable immersion levels. J Comput Nonlinear Dynam 4(3):031003. doi:10.1115/1.3124088
17. Insperger T, Stépán G (2004) Updated semi-discretization method for periodic delay-differential equations with discrete delay. Int J Numer Meth Eng 61(1):117–141. doi:10.1002/nme.1061
18. Insperger T, Stépán G, Turi J (2008) On the higher-order semi-discretizations for periodic delayed systems. J Sound Vib 313(1–2):334–341. doi:10.1016/j.jsv.2007.11.040
19. Jin G, Qi HJ, Cai YJ, Zhang QC (2016) Stability prediction for milling process with multiple delays using an improved semi-discretization method. Mathematical Methods in the Applied Sciences 39(4):949–958. doi:10.1002/mma.3543
20. Li M, Zhang G, Huang Y (2013) Complete discretization scheme for milling stability prediction. Nonlinear Dynam 71:187–199. doi:10.1007/s11071-012-0651-4

21. Xie QZ (2016) Milling stability prediction using an improved complete discretization method. Int J Adv Manuf Technol 83(5–8):815–821. doi:10.1007/s00170-015-7626-9
22. Li Z, Yang Z, Peng Y, Zhu F, Ming X (2015) Prediction of chatter stability for milling process using Runge-Kutta-based complete discretization method. Int J Adv Manuf Technol 86(1):943–952. doi:10.1007/s00170-015-8207-7
23. Ozoegwu CG (2016) High order vector numerical integration schemes applied in state space milling stability analysis. Appl Math Comput 273:1025–1040. doi:10.1016/j.amc.2015.10.069
24. Ding Y, Zhu LM, Zhang XJ, Ding H (2010a) A full-discretization method for prediction of milling stability. Int J Mach Tools Manuf 50(5):502–509. doi:10.1016/j.ijmachtools.2010.01.003
25. Ding Y, Zhu LM, Zhang XJ, Ding H (2010b) Second-order full-discretization method for milling stability prediction. Int J Mach Tools Manuf 50(10):926–932. doi:10.1016/j.ijmachtools. 2010.05.005
26. Ding Y, Zhu LM, Zhang XJ, Ding H (2011) Numerical integration method for prediction of milling stability. J Manuf Sci Eng 133(3):031005. doi:10.1115/1.4004136
27. Liang XG, Yao ZQ, Luo L, Hu J (2013) An improved numerical integration method for predicting milling stability with varying time delay. Int J Adv Manuf Technol 68:1967–1976. doi:10.1007/s00170-013-4813-4
28. Guo Q, Sun YW, Jiang Y (2012) On the accurate calculation of milling stability limits using third-order full-discretization method. Int J Mach Tools Manuf 62:61–66. doi:10.1016/j.ijmachtools.2012.05.001
29. Guo Q, Jiang Y, Zhao B, Ming P (2016) Chatter modeling and stability lobes predicting for non-uniform helix tools. Int J Adv Manuf Technol (on line). doi:10.1007/s00170-016-8458-y
30. Ozoegwu CG (2014) Least squares approximated stability boundaries of milling process. Int J Mach Tools Manuf 79:24–30. doi:10.1016/j.ijmachtools.2014.02.001
31. Ozoegwu CG, Omenyi SN, Ofochebe SM (2015) Hyper-third order full-discretization methods in milling stability prediction. Int J Mach Tools Manuf 92:1–9. doi:10.1016/j.ijmachtools.2015.02.007
32. Tang X, Peng F, Yan R, Gong Y, Li Y, Jiang L (2016) Accurate and efficient prediction of milling stability with updated full-discretization method. Int J Adv Manuf Technol (on line). doi:10.1007/s00170-016-8923-7
33. Long X, Balachandran B (2010) Stability of up-milling and down-milling operations with variable spindle speed. J Vib Control 16(7–8):1151–1168. doi:10.1177/1077546309341131